PCCP

Energetics of high temperature degradation of fentanyl into primary and secondary products

Journal:	*Physical Chemistry Chemical Physics*
Manuscript ID	CP-ART-06-2023-003068.R1
Article Type:	Paper
Date Submitted by the Author:	20-Oct-2023
Complete List of Authors:	Poudel, Bharat; University of Vermont Monteith, Haley; Sandia National Laboratories Sammon, Jason; Sandia National Laboratories Whiting, Joshua; Sandia National Laboratories California Moorman, Matthew; Sandia National Laboratories Vanegas, Juan; University of Vermont Rempe, Susan; Sandia National Laboratories

PCCP

ARTICLE TYPE

Cite this: DOI: 00.0000/xxxxxxxxxx

Energetics of high temperature degradation of fentanyl into primary and secondary products

Bharat Poudel,[a] Haley L. Monteith,[b] Jason P. Sammon,[b] #Joshua J. Whiting,[b] Matthew W. Moorman,[b] Juan M. Vanegas [c,d*], and Susan B. Rempe[e*]

Received Date
Accepted Date

DOI: 00.0000/xxxxxxxxxx

Fentanyl is a synthetic opioid used for managing chronic pain. Due to its higher potency (50-100x) than morphine, fentanyl is also an abused drug. A sensor that could detect illicit fentanyl by identifying its thermally degraded fragments would be helpful to law enforcement. While experimental studies have probed the thermal degradation of fentanyl, little theoretical work has been done to understand the mechanism. Here, we studied the thermal degradation pathways of fentanyl using extensive *ab initio* molecular dynamics simulations combined with enhanced sampling via multiple-walker metadynamics. We calculated the free energy profile for each bond suggested earlier as a potential degradation point to map the thermodynamic driving forces. We also estimated the forward attempt rate of each bond degradation reaction to gain information about degradation kinetics.

1 Introduction

Fentanyl is a powerful synthetic opioid drug used to relieve and manage severe pain. Fentanyl was first synthesized in Belgium in the 1950s and introduced to the USA in 1968 for medical purposes.[1] Fentanyl is often used to treat patients with chronic pain, such as cancer patients and those who are physically intolerant to other opioids.[2] Due to its high potential for abuse and addiction, fentanyl is classified as a Schedule II controlled drug. Fentanyl addiction has become an increasing problem due to its 50-100 times higher potency compared to morphine.[3] Not only is fentanyl in high demand in the market, but so are its derivatives.[4] As an abused drug, fentanyl can be taken through injection, ingestion, and inhalation.[5] Fentanyl poses a threat to homeland security as well as law enforcement personnel because involuntary exposure can cause severe health problems or even death.[6]

Rapid and accurate detection of illicit fentanyl and its various analogs is an ongoing challenge. Detection may be focused on the degradation of fentanyl and its analogs. Different degradation approaches are known to exist for fentanyl, including thermal degradation,[3,7,8] oxidative degradation,[8] acid treatment, and base treatment.[9] Out of all those approaches, thermal degradation is the most studied mode of fentanyl decomposition because it occurs more rapidly and efficiently. In addition to destroying the molecule and aiding in the detection of illicit fentanyl, this degradation method is also important due to the interest in thermally generated aerosols for efficient drug delivery.[10]

A probe that could detect fentanyl from thermally degraded fragments would be a helpful new tool for managing illicit fentanyl. Our goal here is to understand the mechanisms of fentanyl thermal degradation to facilitate the development of such a probe.

Fentanyl decomposes into different products, depending on the degradation processes. A degradation study done under acidic conditions reported that fentanyl degraded to N-phenylpropionamide.[8] While fentanyl remains stable under light, oxidation with hydrogen peroxide produces fentanyl N-oxide.[8] Thermally, fentanyl can be degraded into several compounds under high temperatures in a short period of time.[11] This degradation method was found to be efficient at destroying the compound. The application of heat also leads to the formation of different products, which can be toxic. To avoid the formation of toxic products, it is important to understand the stability of fentanyl at different temperatures and the energetics for the decomposition of fentanyl. To address those issues, here we studied the thermal decomposition pathways of fentanyl using free energy methods.

The thermal decomposition of fentanyl has been studied, especially the pyrolysis of fentanyl and its derivatives (Fig. 1, Table 1). The study by Manral, et al. focused on the toxicity and degra-

*Corresponding authors: vanegasj@oregonstate.edu, slrempe@sandia.gov
[a]Materials Science Graduate Program, The University of Vermont, Burlington, VT USA
[b]Biological and Chemical Sensors, Sandia National Laboratories, Albuquerque, NM USA
[c]Department of Physics, The University of Vermont, Burlington, VT USA
[d]Present address: Department of Biochemistry and Biophysics, Oregon State University, Corvallis, OR USA
[e]Center for Integrated Nanotechnologies, Sandia National Laboratories, Albuquerque, NM USA

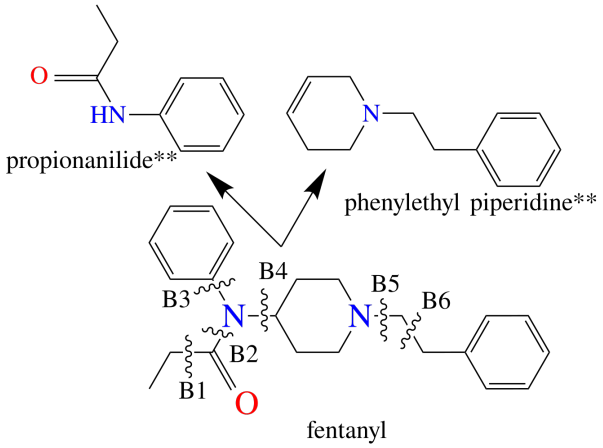

Fig. 1 Fentanyl and some of its commonly observed thermal degradation products. Double asterisk (**) applies to observations made under anaerobic conditions.Table 1 lists compounds formed from the breaking of specific bonds, labeled here as B1 - B6. Arrows identify fragments formed from breaking bond B4.

Table 1 Commonly observed fentanyl thermal degradation fragments

Fragment name	Bond
Despropionyl fentanyl	B2
Propionanilide (PRP	B4
Phenylethyl piperidine (PEP)	B4
Norfentanyl	B5
Pyridine	B4 and B5
Benzyl-X	B6

dation of fentanyl under elevated temperatures.[7] They observed that a high temperature of 750 °C may lead to some toxic compounds, including hydrogen cyanide.[7] They also reported that the aerosol generated by heating fentanyl powder on a hot plate is ∼70% pure, suggesting that ∼30% degraded to other compounds. This result indicates that the duration of heat exposure also plays an active role in degradation.

Manral et al.[7] and Rabinowitz et al.[11] reported that the parent fentanyl was stable up to 350 °C, as suggested by a single peak in their gas chromatography-mass spectrometry (GC-MS) experiments. Two peaks appeared when the temperature was increased to 500 °C, with degradants identified as propionanilide (PRP) and phenylethyl piperidine (PEP), which often undergoes further chemical modification into phenylethyl pyridinium. Further increasing the temperature to 750 °C produced several peaks because the primary degradant PEP was further degraded. The secondary degradation of the fragment PRP has not been reported yet in prior studies to the best of our knowledge. However, the secondary degradation of PEP under high temperature remains unexplained. Nishikawa[12] used fentanyl, and HCl as a salt, and observed benzylchloride as a degradant at 750 °C under aerobic conditions. Garg et al. heated the fentanyl powder for 5 mins under 750 °C and observed its degradation into two known products, propionanilide and norfentanyl,[8] and three unknown degradants that were identified as PEP derivatives.

Nishikawa et al. reported the detection of fentanyl degradation under both aerobic and anaerobic conditions at 750 °C.[3] The fragments produced are propionanilide and norfentanyl under both conditions.[3] Other degradation studies by Lambropoulos et al.[9] and Garg et al.[8] reported that despropionyl fentanyl was formed under aerobic conditions. Other researchers reported similar patterns of fentanyl degradation, but not all agree on the secondary degradation of PEP. The breaking of the B4 bond (Fig. 1) gives rise to propionanilide and PEP. While some studies reported the formation of PEP under low temperature, its charged state was not explained well by the prior studies. Nishikawa did not see PEP as a degradant while Manral et al. observed PEP at 500 °C and Garg et al. observed PEP as a degradant.[8]

Pyridine is also one of the common products observed during thermal degradation. The formation of pyridine was explained by the initial formation of free radicals during elimination cleaving at bonds B4 and B5, as explained by Nishikawa et al.[3] However, Manral et al. explained it as the dehydrogenation of the unsaturated piperidine ring of PEP after the secondary degradation of bond (B5). The presence of a double bond in the piperidine ring of PEP facilitated the dehydrogenation of the molecule to form pyridine.[8]

All studies carried out so far showed that the potential degradation mechanism starts from the bond that is linked with a nitrogen (N) atom[3,7,8,11] However, the cause of bond breaking and the energetics for the bond breaking have not been studied so far. Also, no data have been reported about the degradation of bond B3 made by the N atom. A recent review of fentanyl suggests the need for extending the theoretical work on the fentanyl degradation mechanism.[10] Here, we explore the free energies and kinetics for bond breaking via extensive *ab initio* molecular dynamics (AIMD) simulations and free energy calculations.

2 Materials and Methods

2.1 Pyrolysis

Fentanyl certified standards (1 mg/mL) were procured from Cerilliant (F-013-1ML, Round Rock, TX). Fentanyl in 10 µg volumes was flash pyrolyzed with a Gerstel (Mülheim an der Ruhr, Germany) multi-functional pyrolysis (MPS) system connected to a comprehensive two-dimensional gas chromatograph with high-resolution time-of-flight mass spectrometry (GCxGC-HRMS) from LECO Corporation (Pegasus GC-HRT+ 4D, St. Joseph, MI) with a 10 m length of 0.1 mm DB-WAX capillary column with a 0.2 µm film thickness primary column and a 2 m length of 0.1 mm DB-1 capillary column with a 0.1 µm film thickness both from Agilent (Santa Clara, CA) secondary column installed. The system uses a liquid nitrogen cooled thermal modulator. The temperature of primary column was initially held at 40 °C for 2 minutes and then ramped at 5 °C/min to 225 °C and held here for 4 minutes. The transfer line was held at 275 °C, the electron impact ionization source was set to 70 eV, the source temperature was set to 250 °C. The scan rate for the MS was set to 24 Hz and the mass range was set to 16 to 350 amu. Pyrolysis was performed with a 50 °C initial temperature, and ramped at 260 °C/s to two different final, one-minute holds of 500 and 700 °C. The pyrolysis products were cryo-refocused on a Gerstel CIS inlet held at -100 °C.

This inlet was heated at 12 °C/s to 300 °C to desorb the pyrolysis products into the mobile phase flow path. This temperature was maintained for the duration of the analytical run. Summed peak area percentages of fentanyl fragments were extracted from GCxGC-HRMS raw data. Each temperature condition was analyzed independently. The summed peak area percentages were then averaged by temperature condition. GCxGC-HRMS fentanyl fragment peaks were verified via retention time and visually on the chromatogram.

2.2 AIMD simulations

AIMD simulations were performed using the Quickstep[13] module of the CP2K software package,[14] which performs density functional theory (DFT) calculations with the Gaussian and plane waves method (GPW). The PBE (Perdew–Burke–Ernzerhof) generalized gradient approximation[15] was used for the exchange–correlation functional in the DFT calculations. Wavefunction optimization at each self-consistent field (SCF) step was performed with the orbital transformation method[16] and direct inversion in the iterative subspace method. The optimized double-zeta basis set (DZVP-MOLOPT) was applied to all the atoms together with the Goedecker–Teter–Hutter (GTH) pseudopotentials.[17–20] The geometry of each system was optimized using a conjugate gradient algorithm before running the MD simulation. A time step of 0.5 fs was chosen for dynamics. A Nose-Hoover thermostat was used to keep the temperature constant at 1,273 K. The higher temperature compared to experiments was chosen to accelerate the dynamics due to the limited time scale of the simulations in the ps range. All simulations were run in a constant rectangular cell of dimensions 30 Å × 30 Å × 30 Å. The electrostatic potential (ESP) of the atomic partial charges on the atoms was computed using the Breneman model, which reproduces the molecular electrostatic potential. This model was implemented in Q-Chem[21] as the CHELPG (Charge Extrapolation using the Lagrange Points Grid) method to compute the partial charges.[22] We first optimized the structure using the VDZ (Valence-Double-Zeta) basis set and the PBE (Perdew–Burke–Ernzerhof) generalized gradient approximation[15] for the exchange–correlation functional in the DFT calculations, followed by a single point calculation.

2.3 Free energy calculations

Free energy calculations were performed with CP2K together with the PLUMED plugin.[23,24] To compute the free energy of bond breaking at selected bonds, we first used steered MD with the bond length (d) as the collective variable (CV, also known as a reaction coordinate). A spring constant of 1,000,000 kJ/mol/nm^2 was used for the time-dependent harmonic restraint potential that linearly increases the bond length up to ∼5.5 Å. After running the steered CV simulation, 10 configurations were chosen at uniform intervals along the bond CV and equilibrated for 0.5 ps while holding each bond length fixed with a fixed harmonic potential. We used these 10 configurations to run multiple-walker well-tempered metadynamics to compute the free energy.[25,26] In the metadynamics runs, the simulations are biased with a time-dependent (t) potential of the form,

$$V(d,t) = \sum_{t'}^{t'<t} W \exp\left(-\frac{V(d,t')}{k_B \Delta T}\right) \exp\left(-\frac{(d-d(t'))^2}{2\sigma^2}\right), \quad (1)$$

where W and σ are the height and width of the added Gaussian hills, respectively. Variable ΔT is a fictitious maximum increase in temperature that ensures convergence by limiting the extent of the free energy exploration. At long timescales, the unbiased free energy, $G(d)$, can be recovered from

$$V(d,t\to\infty) = -\frac{\Delta T}{T+\Delta T} G(d) + C, \quad (2)$$

where C is an immaterial constant. The value of ΔT is set by the 'bias factor' parameter, $B = \frac{T+\Delta T}{T}$, and the frequency of addition of Gaussian hills is determined by a fixed deposition rate, ω. The same values of $\sigma = 0.01$ Å, $B = 15$, $W = 5.3$ kJ/mol, and $\omega = 30$ fs were used for all free energy calculations. All walkers were then simultaneously run for >15 ps each using well-tempered metadynamics. Therefore, the combined simulation time to obtain each free energy surface was >150 ps (10 walkers × 15 ps). Convergence of the free energy profiles was monitored by computing the difference between the minimum (G_{min}, at the equilibrium bond length) and the maximum (G_{max}, at the transition barrier) free energy values in 2 ps intervals (per walker). All figures were plotted using the Matplotlib library.[27]

3 Results and Discussion

3.1 Degradation Pathways of Parent Fentanyl

We initially focus on exploring the different degradation pathways of fentanyl by characterizing the free energy required for breaking specific bonds of interest. We choose four (4) different bonds in the vicinity of the two N atoms in fentanyl. Previous experimental pyrolytic studies[3,7,8] determined that fragmentation is most likely at the N-C bonds, particularly near the piperidine ring.

We compute the free energy of bond breaking in *ab initio* molecular dynamics (AIMD) simulations by stretching a particular bond using a steered harmonic potential until the atoms are no longer bonded, followed by a well-tempered metadynamics simulation (see Methods). We estimate the free energies of bond breaking through metadynamics as it includes important entropic effects[28,29] and efficient configurational sampling in contrast to the more conventionally used relaxed scanning of the potential energy surface. Since fentanyl is reported to be photostable,[30] we have only studied the ground electronic state. Note that each bond breaking reaction is characterized by an energy saddle with a maximum energy barrier at the transition state.

Fig. 2A shows the free energy profiles of bond breaking for the four selected N-C bonds of fentanyl (B2 through B5). The lowest free energy barrier is for B4 (shown in blue), with a value of ∼105 kJ/mol at 1,000 °C. This result suggests that the most likely primary degradation products of the parent fentanyl are propionanilide (PRP) and phenylethyl piperidine (PEP). This pathway (Fig. 1) is in agreement with previous experimental studies that show the occurrence of these degradation products.[3,7,8]

Table 2 Experimentally observed fentanyl degradation products.

Ref.	Rate	Exposure time	Final T (°C)	Fragments
Nishikawa[3]	20 °C/s	10 s	750	PRP and X*
Garg**[8]	-	5 min	350	PRP, NRF and PEP derivatives
Manral[7]	-	-	500	PRP and PEP
Manral[7]	-	-	750	PRP derivatives
This work	260 °C/s	1 min	500	PRP, PEP derivatives
This work	260 °C/s	1 min	700	PRP, PEP derivatives

PRP = propionanilide; X* = benzylaldehyde, despropionyl fentanyl, pyridine, styrene; NRF = norfentanyl; PEP = phenylethyl piperidine and/or phenylethyl pyridinium. **Garg observed fentanyl degrade to despropionyl fentanyl under acidic conditions

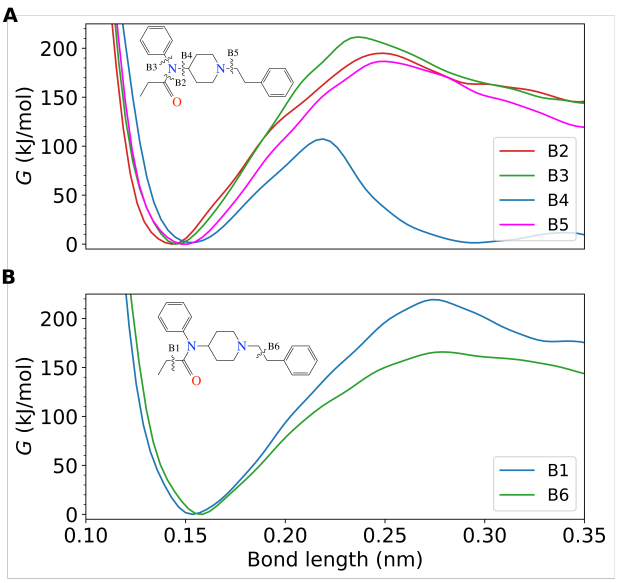

Fig. 2 Free energy profiles of bond breaking in fentanyl predicted by enhanced sampling *ab initio* simulations (1,000 °C). Free energy is estimated using well-tempered metadynamics with the bond distance between atoms as the reaction coordinate. Panel A shows bonds between N and C atoms, while panel B shows neighboring C–C bonds for comparison.

In contrast to the low energy barrier observed for B4, the energy required to break the bonds at B2 and B3 is much higher, with barriers of 195 and 212 kJ/mol respectively (Fig. 2A). These two bonds have significantly higher energy despite also being N-C bonds and being connected to the same nitrogen atom. The degradation of bond B2 gives rise to despropionyl fentanyl, which has been observed in pyrolytic studies. Earlier studies have not reported any products that arise from the degradation of B3. The higher energy needed to break bonds B2 and B3 is also reflected by the larger bond length associated with the barrier.

Bond B5, involving the second nitrogen atom in fentanyl, shows a high barrier (186 kJ/mol), similar to B2 and B3. Breaking of fentanyl at B5 results in norfentanyl, which has also been observed in pyrolytic studies.[8]

In addition to the N-C bonds, we also studied two nearby C-C bonds at B1 and B6 for comparison (Fig. 2B). Degradation at B6 has been observed in previous studies.[10,12] Nishikawa reported that breaking at B6 gives rise to benzyl-X[12], where the halide ion, X, is Cl^- in this case. The energy barriers for degradation at B1 (219 kJ/mol) and B6 (166 kJ/mol) are of the same order of magnitude as the other N-C bonds (Fig. 2B).

Results thus far reported in earlier experimental studies for fentanyl degradation, as well as our experimental findings reported here, show that the primary degradation path leads to the formation of PEP (Table 2). Those experimental works show that a high rate of increase in temperature requires less exposure (1 min) in order to degrade the parent fentanyl. We have increased the temperature to 500 °C and 700 °C, and find the same primary fragments, along with evidence of secondary degradation of the primary fragments (see Table 1 and Fig. 1 in the Supplementary Material).

Our free energy calculations predict that the N-C bond has the lowest free energy and, therefore, it would be the most likely one to break (Fig. 2). Previous experiments and our own GC-MS results show that fentanyl breaks into PEP and PRP under heating, in agreement with our free energy predictions. However, experiments also predict formation of other smaller fragments while our energetics of primary degradation suggest that the formation of those fragments would have high energies. Therefore, the molecule may be forming these smaller fragments through secondary degradation processes. To gain more insight about these experimental results, we explored this secondary degradation reaction, as reported in the following section.

3.2 Secondary Degradation of Fentanyl

In the previous section, we described our investigations of the primary degradation of the parent fentanyl at various bonds within the molecule. However, our free energy calculations do not provide a complete picture because these primary products may further degrade into secondary ones, as suggested by experiments. To address that possibility, we explore secondary degradation of the PEP primary product through a similar approach as taken before. Assuming that both the N and C atoms around B4 take one unpaired electron during the breaking of this bond in the parent fentanyl molecule, the resulting PEP-like fragment will be a negatively-charged free radical (Fig. 3. This charged free-radical state may have important consequences on the overall stability of the molecule and, therefore, degradation may happen more readily compared to the parent fentanyl.

Calculation of the partial charges (see Methods) for atoms near the nitrogen for each of the secondary reactants shows significant

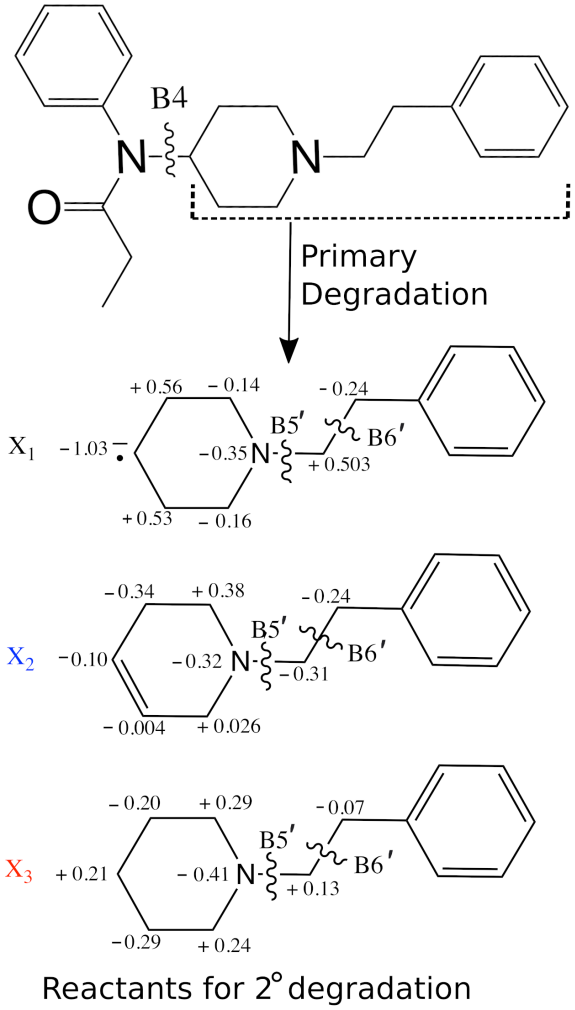

Fig. 3 Three possible chemical configurations are considered for secondary degradation based on the bonding of the pyridine ring: 1) a negatively charged free radical (X_1), 2) neutral, with a double bond to one of the adjacent C (X_2), and 3) neutral, with a single bond to the adjacent C (X_3). The number of H atoms were adjusted in cases 2 and 3 to match the type of C-C bond. Partial charges obtained with the CHELPG method from a single point calculation after energy minimization are shown for selected atoms near the pyridine ring for each structure (see Methods).

variation, not only in the atoms of the pyridine ring, but also along the atoms between the B5' and B6' bonds (Fig. 3). The ~ -1 charge on the carbon opposite to the N in the ring indicates that the unpaired electron is localized at this atom in the free-radical anion (X_1).

We estimate the free energy profile for degradation of the free radical PEP-like anion (X_1) at bonds 5 and 6, labeled as B5' and B6' to avoid confusion (Fig. 3). In addition to the free radical reactant, we also estimate the free energy of breaking bonds B5' and B6' in two possible neutral reactants: 1) after the further loss of a proton in the pyridine ring to form a C-C double bond (labeled X_2 in Fig. 3), and 2) after acquiring a proton to neutralize the charged free radical (labeled X_3 in Fig. 3). Our experimental results show that the primary degradation produces PEP-like products under both 500 °C and 700 °C. These primary degradation

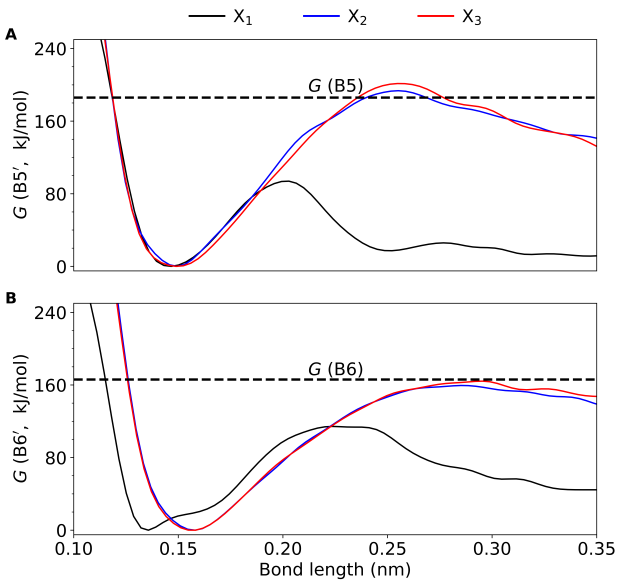

Fig. 4 Free energy profiles of secondary degradation in the PEP-like fentanyl fragments at 1,000 °C. Panel A shows data for bond breaking between N and C atoms (B5'), while panel B shows data for bond breaking at the neighboring C–C bond (B6'). Dashed lines show the maximum free energy barrier observed for the same bond during primary degradation in the parent fentanyl molecule. Free energy was estimated using well-tempered metadynamics, with the bond distance between atoms as the reaction coordinate.

products then undergo secondary degradation to produce other fragments, such as toluene and pyridine (see Methods for detailed experimental setup and SI for more experimental results).

We find that the free energy for breaking the bonds at B5' (Fig. 4 a) and B6' (Fig. 4b) remains practically unchanged for the neutral PEP-like reactants compared to the parent fentanyl (black dashed lines). In contrast, the free energy barrier for breaking B5' and B6' for the PEP-like free radical anion is significantly lower than the free energy of degradation of these same bonds in the parent fentanyl (Fig. 4). These results suggest that, once the parent fentanyl degrades, the secondary degradation most likely happens in the charged free radical state. The lower free energy barriers for breaking the PEP-like free radical molecule at B5' and B6' would facilitate the formation of compounds, such as toluene and pyridine, through secondary degradation processes.

3.3 Estimated kinetics from attempt rates

Capturing rare events that describe the entire kinetics of bond breaking may not be possible. Also, computational expense may prohibit computation of transitions between the reactant and product states. To overcome those challenges, we estimate the kinetics of the bond breaking on the basis of the free energy barrier at the transition state and dissociation time. We use an Arrhenius-Bell model to estimate the forward attempt rate, which refers to the probability of reactants crossing the free energy barrier.[31,32] The attempt rate can be estimated using

$$k_f = \frac{1}{t_D} \exp\left(\frac{-\Delta G^{\dagger}}{k_B T}\right), \quad (3)$$

where t_D is the diffusive relaxation time, $\Delta G^\dagger$ is the difference in free energy between reactants and the transition state, k_B is the Boltzmann constant and T is the temperature. The diffusive relaxation time is the inverse of the bond vibrational frequency and it is computed by quantifying the temporal variations in bond distances during the equilibrium (unbiased) simulations. We used Fourier analysis to extract the frequencies associated with these bond fluctuations.[33]

The forward attempt rate, k_f, depends on the spontaneous dissociation rate and on the difference in the free energy between the two states (reactant and transition states). Since k_f is exponentially related to the free energy difference, as shown in Eq. 3, even a small change in free energy changes k_f significantly. We calculate the ratio of the forward attempt rate of all bonds to the forward attempt rate of B4 (k_f/k_f (B4)) to estimate the likelihood of bond breaking. Bonds B3 and B1 are less likely to break, followed by B5, B2 and B6. Bonds B5' and B6' are more likely to break in the negative charged state (Table 3).

Table 3 Dissociation time, free energy barrier, and attempt rate

Bond	t_D (ps)	$\Delta G^\dagger$ (kJ/mol)	k_f (s^{-1})	k_f/k_f(B4)
B1	31.6	219 ± 2.1	3.1×10^1	2.2×10^{-5}
B2	39.4	195 ± 2.8	2.6×10^2	1.8×10^{-4}
B3	49.7	212 ± 3.7	4.1×10^1	2.9×10^{-5}
B4	34.8	105 ± 1.72	1.4×10^6	1
B5	30.7	186 ± 1.35	7.1×10^2	5.1×10^{-4}
B6	34.1	166 ± 0.87	4.5×10^3	3.2×10^{-3}
B5'	32.1	93 ± 2.7	4.7×10^6	3.35
B6'	26.7	114 ± 3.87	6.5×10^5	0.46

4 Conclusion

We have elucidated the degradation pathway followed by the parent fentanyl, as well as by the primary degradant (PEP), through free energy calculations and GC-MS experiment. The theoretical results provide additional insights that support the appearance of both primary and secondary degradation products experimentally. Specifically, the predicted free energy pathway for fentanyl degradation shows that the bond formed by nitrogen, outside the pyridine ring, to the nearest carbon in the pyridine ring (bond B4) is the primary site for initial bond breaking. That bond has the lowest free energy barrier, 105 kJ/mol, suggesting this bond breaks more easily than the others, which agrees with prior experimental observations.[3,7,8] Comparing free energy barriers, the ease of bond breaking follows this order: B4, B6 (166 kJ/mol), B5 (186 kJ/mol), B2 (195 kJ/mol), B3 (212 kJ/mol) and B1 (219 kJ/mol).

While the secondary degradation of fentanyl was observed earlier in experiments, the pathway was not examined. To gain insight into the secondary degradation, we studied PEP in three different structures: two in neutral conditions that differ by bonding between adjacent carbons, and one in a free radical negatively charged state. Based on our calculations of free energy, we find that the secondary degradation reaction likely only happens in the PEP-like free radical anion. The free energy barrier for breaking bonds B5' and B6' in this free radical are 93 kJ/mol and 114 kJ/mol, respectively.

The results of our theoretical and experimental investigation support the degradation pathways reported by earlier experiments. By providing the first free energy analysis of both primary and secondary degradation pathways, this work also identifies probable bond-breaking sites and resulting products. This work lays the foundation for future studies of the thermal degradation pathways of fentanyl analogues, such as furanyl fentanyl and acetyl fentanyl.

5 Acknowledgments

We gratefully acknowledge funding from the Department of Defense. This work was performed, in part, at the Center for Integrated Nanotechnologies, an Office of Science User Facility operated for the U.S. Department of Energy (DOE) Office of Science. Computations were performed, in part, on the Vermont Advanced Computing Core supported in part by NSF Award No. OAC-1827314.

The authors declare no competing financial interest.

Notes and references

1 K. Hasegawa, K. Minakata, M. Suzuki and O. Suzuki, *Forensic Toxicol.*, 2022, **40(2)**, 234–243.
2 L. Nelson and R. Schwaner, *J. Med. Toxicol.*, 2009, **5(4)**, 230–241.
3 R. K. Nishikawa, S. C. Bell, J. C. Kraner and P. S. Callery., *J. Anal. Toxicol.*, 2009, **33(8)**, 418–422.
4 H. Schumann, T. Erickson, T. M. Thompson, J. L. Zautcke and J. S. Denton, *Clin. Toxicol.*, 2009, **46(6)**, 501–506.
5 P. W. Moore, R. B. Palmer and J. W. Donovan., *J. Forensic Sci.*, 2014, **60(1)**, 243–246.
6 D. E. A. US Department of Justice, *National Drug Threat Assessment*, 2019.
7 L. Manral, P. K. Gupta, M. V. S. Suryanarayana, K. Ganesan and R. C. Malhotra, *J. Therm. Anal. Calorim.*, 2009, **96**, 531–534.
8 A. Garg and D. W. Solas and L. H. Takahashi and J. V. Cassella, *J. Pharm. Biomed. Anal.*, 2010, **53 (3)**, 325–334.
9 J. Lambrolous, G. A. Spanos, N. V. Lazaridis, T. S. Ingallinera and V. K. Rodriguez., *J. Pharm. Biomed. Anal*, 1999, **4**, 705–716.

10 M. Bazley, M. Logan, C. Baxter, A. A. B. Robertson and J. T. Blanchfield., *Aus. J. Chem.*, 2020, **10**, 868–879.

11 J. D. Rabinowitz, M. Wensley, P. Lloyd , D. Myers, W. Shen, A. Lu, C. Hodges, R. Hale, D. Mufson, A. Zaffaroni, *J. Pharmacol. Exp. Ther.*, 2004, **309(2)**, 769–775.

12 R. K. Nishikawa, *PhD thesis*, West Virginia University, 2012.

13 V. J, M. Krack, F. Mohamed, M. Parrinello, T. Chassaing and J. Hutter, *Comput. Phys. Commun.*, 2005, **167**, 103–128.

14 D. Kühne, M. Iannuzzi, M. D. Ben, V. Rybkin, P. Seewald, F. Stein, T. Laino, R. Z. Khaliullin, O. Schütt, F. Schiffmann, D. Golze, J. Wilhelm, S. Chulkov, M. Bani-Hashemian, V. Weber, U. Borštnik, M. Taillefumier, A. S. Jakobovits, A. Lazzaro, H. Pabst, T. Müller, R. Schade, M. Guidon, S. Andermatt, N. Holmberg, G. Schenter, A. Hehn, A. Bussy, F. Belleflamme, G. Tabacchi, A. Glöß, M. Lass, I. Bethune, C. J. Mundy, C. Plessl, M. Watkins, J. VandeVondele, M. Krack and J. Hutter, *J. Chem. Phys.*, 2020, **152**, 194103.

15 J. Perdew, K. Burke and M. Ernzerhof, *Phys. Rev. Lett.*, 1996, **77**, 3865–3868.

16 J. VandeVondele and J. Hutter, *J. Chem. Phys.*, 2003, **118**, 4365–4369.

17 J. VandeVondele and J. Hutter, *J. Chem. Phys.*, 2007, **127**, 114105.

18 S. Goedecker, M. Teter and J. Hutter, *Phys. Rev. B*, 1996, **54**, 1703–1710.

19 C. Hartwigsen, S. Goedecker and J. Hutter, *Phys. Rev. B*, 1998, **58**, 3641–3662.

20 M. Krack, *Theor Chem Account*, 2005, **114**, 145–152.

21 Y. Shao *et al.*, *Mol. Phys.*, 2014, **113**, 184–215.

22 C. M. Breneman and K. B. Wiberg, *J. Comput. Chem.*, 1990, **11**, 361–373.

23 M. Bonomi, D. Branduardi, G. Bussi, C. Camilloni, D. Provasi, P. Raiteri, D. Donadio, F. Marinelli, F. Pietrucci, R. A. Broglia and M. P. , *Comput. Phys. Commun.*, 2009, **180**, 1961–1972.

24 G. A. Tribello, M. Bonomi, D. Branduardi, C. Camilloni and G. Bussi, *Comput. Phys. Commun.*, 2014, **185**, 604–613.

25 P. Raiteri, A. Laio, F. L. Gervasio, C. Micheletti and M. Parrinello, *J. Phys. Chem. B*, 2006, **110**, 3533–3539.

26 A. Barducci, G. Bussi, and M. Parrinello, *Phys. Rev. Lett.*, 2008, **100**, 020603.

27 J. D. Hunter, *Comput. Sci. Eng.*, 2007, **9**, 90–95.

28 F. Yue, B. Leonardo and l. Peng, *J. Am. Chem. Soc.*, 2021, **143**, 1577–1589.

29 K. R. Gorantla and B. S. Mallik, *J. Phys. Chem. A*, 2020, **124**, 836–848.

30 J. Trawiński, P. Szpot, M. Zawadzki and R. Skibiński, *Sci. Total Environ.*, 2021, **791**, 148171.

31 J. Vanegas and M. Arroyo, *PLoS ONE*, 2014, **9(12)**, 1–22.

32 E. Evans, *Annual Rev. Biophys. Biomol. Struct.*, 2001, **30**, 105–128.

33 S. B. Rempe and H. Jónsson, *Chem. Educ.*, 1998, **3**, 1–17.